# Underthrusting of the Tarim lithosphere beneath the western Kunlun range, insights from seismic profiling evidence

Shengli Wang, Yan Chen, Julien Charreau, Yongxiang Li, Zhuxin Chen, Guangyou Zhu, Huaizhi Xu, Chao Li, Liangshu Wang

# Underthrusting of the Tarim lithosphere beneath the western Kunlun range, insights from seismic profiling evidence

**Shengli Wang[1], Yan Chen[2], Julien Charreau[3], Yongxiang Li[1], Zhuxin Chen[4], Guangyou Zhu[4], Huaizhi Xu[1], Chao Li[1] and Liangshu Wang[1]**

[1]School of Earth Sciences and Engineering, Institute of Continental Geodynamics, Nanjing University, Nanjing, Jiangsu, 210046, China

[2]Univ. Orléans, CNRS, BRGM, ISTO, UMR 7327, F-45071, Orléans, France

[3]Centre de Recherche Pétrographique et Géochimique, 15 rue Notre Dame des Pauvres, B.P. 20, 54501 Vandoeuvre lès Nancy, France

[4]Research Institute of Petroleum Exploration & Development, PteroChina, Beijing 10083, China

Corresponding author: ShengLi Wang (wangsl@nju.edu.cn)

**Key Points:**

- Underthrusting of the Tarim lithosphere beneath the western Kunlun range at ~8.18 mm/yr persisted since ~30 Ma.
- Growth of the western Kunlun range slightly predated ~40 Ma.
- The Tarim Basin was ponded by the Himalayan-Tibetan and Tian Shan orogens since ~25 Ma.

This article has been accepted for publication and undergone full peer review but has not been through the copyediting, typesetting, pagination and proofreading process, which may lead to differences between this version and the Version of Record. Please cite this article as doi: 10.1029/2019TC005932.

**Abstract**

Uplift of the western Kunlun range results from the Indian indentation into Eurasia and induced underthrusting of the Tarim lithosphere. This underthrusting keeps pace with migration of the western Kunlun foreland basin. The basin-scale sequences provide a decipherable record of the migration. To quantify the underthrusting, we analyzed a ~323.2-km-long seismic profile crossing the middle segment of the western Kunlun foreland. We traced seismic reflectors to investigate the architecture of the foreland sequences, and assigned ages of reflectors by correlating them with the dated outcropping sections. The foreland sequences consist of four layers. The lowermost Layer 1 starts to lap on the pre-foreland unit at ~40 Ma, indicating that the Cenozoic western Kunlun initiated slightly prior to ~40 Ma. Layer 2 shows a large sharp step northward to exceed the forebulge at ~25 Ma, suggesting that the modern geomorphology of the Tarim Basin took shape. The southwestern boundary of Layer 4 migrates northeastwards by a fold row relative to that of Layer 3. The gradual retreat of reflector terminations from ~40 Ma to ~30 Ma suggests that the Tarim lithosphere is viscoelastic. The linear fitting of the forelandward envelop of reflector termination sites since ~30 Ma indicates that the Tarim lithosphere underthrusted at an average rate of ~8.18 mm/yr. This rate comprises the shortening rate of ~3.8–5.7 mm/yr and the western Kunlun latitudinal propagation rate of ~4.4–2.5 mm/yr. The abrupt increase in sedimentation rate since ~11 Ma suggests that western Kunlun had reached its current elevation.

## 1 Introduction

Continental underthrusting is one of mechanisms of growth of the Tibetan Plateau (Meyer et al., 1998; Tapponnier et al., 2001). Quantifying it over the tens-of-millions-year time scale remains challenging. For the Indian subcontinent that is currently connecting with the active Indian Ocean mid-ridge, its underthrusting rates can be estimated by sea floor magnetic lineations (Molnar and Tapponnier, 1975). Yet, for parts of the Asian continent which passively underthrusted southwards beneath the Tibetan Plateau in the context of the India-Asia collision (Meyer et al., 1998; Gao et al., 2000; Kao et al., 2001; Tapponnier et al., 2001), this method is inapplicable since a continental underthrusting generally causes a synchronous forelandward migration of the foreland basin system overlying the underthrusted lithosphere (Beaumont, 1981; Jordan, 1981; Karner and Watts, 1983). The sedimentary sequences deposited within the foreland basin system, especially within the distal part of the foredeep depozone, gradually lap on the forebulge (DeCelles and Giles, 1996; DeCelles and DeCelles, 2001; Naylor and Sinclair, 2008; DeCelles, 2012; Sinclair and Naylor, 2012). Thus, the infilling sequences of the basin offer a complete, decipherable record of migration of a foreland basin system. Besides understanding continental underthrusting, foreland basin infilling sequences could also provide a means to estimate the uplift of the coupled collisional orogen (Wang et al., 2013).

Here, we present a prime example in Central Asia (Figure 1a) where the Tarim lithosphere is underthrusting beneath western Kunlun, and the underthrusting history is archived in the infilling sequences in the foreland basin. Detailed analysis of the subsurface sedimentary architecture of the infilling sequences using seismic exploration data for hydrocarbon industry, together with well-logging data, and magnetostratigraphic studies (Bosboom et al., 2014a; Zheng et al., 2015), reveals the foreland basin migration process and the initial uplift of western Kunlun. This study would shed new light on hotly debated questions, such as timing of the uplift of Western Kunlun, ponding of the Tarim Basin as well as southward underthrusting rates of Tarim Block under the western Kunlun range.

## 2 Geological setting

Western Kunlun, a ~700-km-long mountain range forming the northwestern border of the Tibetan Plateau, has an average elevation of ~5500 m, and the summits are higher than 7500 m. Western Kunlun originated from a subduction-accretion orogen during Carboniferous time to late Triassic time (Pan, 1990; Hsǜ et al., 1995; Deng, 1996; Matte et al., 1996; Yin and Harrison, 2000; Xiao et al., 2002; 2003). On the closing of the Paleotethys Ocean between the northern Kunlun and Karakoram-Qiangtang block, the western Kunlun collisional orogeny occurred (Yin and Harrison, 2000; Xiao et al., 2002; 2003). Continuous northward docking of Gongwanan blocks in the Jurassic–Early Cretaceous caused the reactivity of the range (Yin, 2010; Cao et al., 2015) to form a foreland basin north of this range. The present topography of western Kunlun resulted from the Cenozoic reactivation of the ancient orogenic belt (Tapponnier and Molnar, 1979; Tapponnier et al., 1982; Avouac and Tapponnier, 1993; Yin and Harrison, 2000; Yin et al., 2010) in the context of the India-Eurasia collision (Molnar and Tapponnier, 1975; Patriat and Achache, 1984). Previous studies characterized the western Kunlun foreland fold-and-thrust belt in terms of its geometry, active thrusting and folding (e.g., He et al., 2016; Lu et al., 2016; Guilbaud et al., 2017). Geophysical surveys indicate that the Tarim lithosphere dips to the south, and extends beneath western Kunlun (Gao et al., 2000; Kao et al., 2001). They attest that the underthrusting of the Tarim lithosphere produced, and is producing the uplift of the western Kunlun range, which is caused by the collision (e.g., Gao et al., 2000; Kao et al., 2001; Cowgill, 2010). The Tarim block was a rifting area in the Paleozoic and deformed as a rigid block in the Mesozoic and the Cenozoic (Jia et al., 1997; Wang and Shen, 2020). A significant fraction of the underthrusting is accommodated by the northward propagation of western Kunlun and crustal shortening along the northeastern piedmont of this range (Lu et al., 2016; Guilbaud et al., 2017). The underthrusting also caused flexure of the Tarim lithosphere to generate the Cenozoic western Kunlun foreland basin (Yin et al., 2002; Jiang et al., 2013).

The foreland basin accommodated up to 10 km thick strata (Jia et al., 2004; Zhang et al., 2004). These strata consist, in an ascending order, of the Paleocene–Eocene Kashi Group (subdivided into the Aertashi, Qimugen, Kalataer, Wulagen and Bashibulak Formations from the bottom up), the Oligocene–middle Miocene Wuqia Group (subdivided into the Keziluoyi, Anjuan and Pakabulak Formations), the middle Miocene–middle Pliocene Artux Formation and the middle Pliocene–Quaternary Xiyu Formation (Figure 2) (Xinjiang BGMR, 1993; Jia et al., 2004; Zhang et al., 2004; Wang and Peng, 2013; Lu et al., 2013; Bosboom et al., 2014a; Zheng et al., 2015). These strata are underlain by Paleozoic and Mesozoic strata (Xinjiang BGMR, 1993; Zhang et al., 2004; Lu et al., 2013; Wang and Peng, 2013).

To the north of the Tarim Basin is Tian Shan. Tian Shan is a Paleozoic orogen (Charvet al., 2011), and reactivated in the Mesozoic (Chen et al., 2011; Wang et al., 2013) and Cenozoic (Tapponnier and Molnar, 1979; Avouac et al., 1993; Yin et al., 1998; Yin, 2010; Wang et al., 2013). Western Tian Shan collided with Pamir at the western corner of the Tarim Basin that caused the ponding of the Tarim Basin.

Our study focused on the middle segment of the western Kunlun foreland through the Bauchu uplift, covered by the Taklimakan sand sea (Figure 1b). In the range front, four rows of fold anticlines have been recognized (Wang and Peng, 2013). The Bachu uplift, also named the central Tarim uplift, is a Cenozoic structural high (Jia, 1997; Jia et al., 2004). Morphological analysis of nine levels of incised fluvial terraces and alluvial fans crossing a fold in conjunction with their age constraints produces a long-term slip rate of 2 to 2.5 mm/yr on its underlying blind ramp (Guilbaud et al., 2017). A seismic profile approximately perpendicularly crossing the middle segment of the western Kunlun foreland images structures and the architecture of the infilling sequences (Figures 3, 4 and S1), which is the target of this study.

## 3 Materials and methods

### 3.1 Materials

We present a seismic profile (Figures 3, 4 and S1), and a borehole stratigraphic column in the western Kunlun foreland area. The seismic investigations were carried out and processed by Tarim Oilfield of PetroChina. These data were provided to Nanjing University for scientific purposes under a scientific agreement by Tarim Oilfield. The seismic profile is pre-stacked migration seismic one that has undergone static and dynamic corrections. The seismic profile image well; and some geologic features imaged in it have been confirmed by the exploration and development of Tarim Oilfield. Therefore, it is a high-quality, credible petroleum industry seismic profile. The seismic profile, trending northeast, begins from the Fusha-Keliyang (F-K) anticline in the southwest, crosses the east of the Yecheng city, the Jade anticline and the Qiaokatage homocline, and ends at the central Tarim Basin in the northeast (Figures 1b, 3 and 4). The profile is ~323.2 km in length, and 7.5 sec of two-way travel time in depth.

Borehole K is located at the crest of the F-K anticline, and ~1 km east of the seismic profile (Figure 1b). This borehole was drilled through the Xiyu and the Artux formations, the Wuqia, and Kashi groups, and ended in the Mesozoic at the depth of 6580.0 m. Figure 5 shows the stratigraphy of this borehole column. VSP logging data and synthetic seismograms were used to correlate formation boundaries to seismic reflectors. And boundaries of Paleozoic strata were calibrated with well-logging data from the Bachu uplift.

3.2 Methods

We employed contractional fault-related folding theories (Shaw et al., 2004), and the kink method to interpret the geometries of folds imaged in the seismic profile (Figs 3 and S1). The subsidence space of the western Kunlun foreland basin is recorded by infilling sedimentary sequences. Well-imaged seismic profiles (Figs 3 and S1) can reveal the sedimentary sequences. Seismic reflectors among Mesozoic and Cenozoic strata imaged in the profile were traced (Figures 3, 4 and S1) to identify their terminations. The seismic profile images Paleozoic marine strata well (Figures 3 and S1), and therefore reflectors among them can be traced unambiguously. Mesozoic and Cenozoic strata are mainly of terrestrial sequences, and the continuity of an individual reflector among them is relatively poor. However, an assemblage of several reflectors is unique, and extends continuously. Thus, we simultaneously delineated a unique assemblage consisting of several reflectors in Mesozoic and Cenozoic strata. We traced a total of 211 reflectors (Figures 4 and S1; Table S1) in the entire profile.

The stratigraphic column (Figure 5) was correlated with the Kekeya magnetostratigraphic section (Zheng et al., 2015), and the Aeratshi section (Bosboom et al., 2014 a), based on the consistent lithology transitions, a growth unconformity, and a marker bed to constrain the ages of the foreland basin sequences.

**4 Results**

4.1 Structures imaged by the seismic profile

The southwestern segment of the profile images the F-K, Kekeya, and Guman anticlines (Figures 3a 4a and S1). The F-K anticline is made up of three thrust sheets. The upper sheet includes Permian, Mesozoic, and Cenozoic strata. The middle sheet comprises Permian and Mesozoic strata. Its roof thrust is located between Mesozoic and Cenozoic strata, and its bottom thrust occurs in Permian mudstone. The lower sheet is composed of Paleozoic rocks. Its bottom fault dips southwestwards, and thrusts northeastwards. The Kekeya anticline is a duplex structure including three thrust sheets. Their roof thrust was formed between Mesozoic and Cenozoic beds, and their floor thrust was produced along Permian mudstone. At the front limb, the floor thrusts cut upwards into Permian and Mesozoic strata, and merge with the roof thrust. The Guman anticline is a wedge structure. At its southwestern limb, the Mesozoic strata pinch out, and the roof thrust occurs in the lower part of the Paleocene evaporite bed. Its floor fault thrusts upwards, cuts Permian strata, and merges with the roof thrust at its northeastern limb to form a decollement fault, termed the Yecheng-Hetian decollement fault (YHD).

The YHD occurs along the gypsum-rich layer at the base of Paleocene strata, and extends northeastwards to the Qiaokatage homocline, and steps upwards to the ground surface to form the Qiaokatage-Mazatage thrust ramp (QMT). The slip along the YHD causes buckling of the hanging wall to form the Jade anticline (Figures 3b, 4band S1). The slip along the bend between the YDH and the QMT produces folding of the hanging wall to form the Qiaokatage homocline.

The high-angle fault below the QMT is the Qiaoka fault. Paleozoic strata of the hanging wall of the Qiaoka fault are slightly thicker than its footwall (Figures 3b, 3c, and S1), suggesting that the Qiaoka fault was a normal fault in the Paleozoic, and inverted to a reverse fault in the Cenozoic (SI text).

The Selibuya fault is ~15 km northeast of the Qiaoka fault and the QMT. It cuts upwards in the middle part of the Artux Formation, and penetrates downwards through the profile. The vertical separation of the Permian base is ~1.1 sec of two-way travel time (~2750 m; the average interval speed of Paleozoic strata is ~5000 m/sec). Reflectors of the lower part of the Artux Formation near the Selibuya fault in the southwestern wall are steeply tilted southwestwards. The middle part of the Artux Formation overlies the Selibuya fault and the tilted lower part of the Artux Formation. The thickness of the Permian and Cambrian strata at the hanging wall of the Selibuya fault is ~1.68 sec (~4200 m), and its thickness at the footwall is ~1.63 sec (~4075 m), indicating that this fault was also normal in the Paleozoic and inverted in the Cenozoic (SI text). The Bachu uplift controlled by the Selibuya fault is a basement-involved structure (Figures 3c, 4c and S1).

A small-scale normal fault is located at ~12 km northeast of the Selibuya fault, and another two antithetic normal faults at ~20 km north of the Selibuya fault. Reflectors between them form a pop-up structure (Figures 3c, 4c and S1), the top of which was eroded and unconformably covered by the middle part of the Artux Formation.

### 4.2 The middle Eocene-Quaternary foreland unit

Based on thickness variation, unconformities, and their associated structures, the sedimentary strata imaged in the seismic profile (Figures 3, 4 and S1) are divided into four tectonostratigraphic units in an ascending order: (a) the Paleozoic rift, (b) the Jurassic–Cretaceous foredeep, (c) the Paleocene–early Eocene continental platform, and (d) the middle Eocene–Quaternary foreland tectonostratigraphic units (SI Text). Given that the filling sequence of the foreland basin records the Cenozoic underthrusting of the Tarim lithosphere, we only finely depicted the architecture of the middle Eocene–Quaternary foreland unit.

This unit accounts for the most thickness of the southwestern segment of the profile, and gradually decreases northeastwards (Figures 3, 4 and S1). The southwestern part of the unit constructs the western Kunlun fold-and-thrust belt. To the northeast of the Kekeya anticline, this unit is well imaged, and reflectors among it can be unambiguously identified. However, to the southwest of the Kekeya anticline, the Cenozoic strata dip at high angles, and are poorly imaged (Figures 3a, and S1). We have traced 157 reflectors in this unit (Figure S1 and Table S1 in SI), containing the Wulagen, Bashibulak, Keziluoyi, Anjuan, Pakabulak, Artux, and Xiyu Formations from bottom up, and identified 135 terminations due to the sedimentary pinch-out, and examined them in detail to decipher the architecture of this unit. For each formation, we delineate seismic reflectors according to their termination orders from southwest to northeast (SI Text).

This middle Eocene–Quaternary foreland tectonostratigraphic unit consists of all the reflectors above R23' (Figures 4 and S1; Table S1). The seismic profile explicitly demonstrates that almost all the reflectors terminate to the foreland (northeastwards), and to the hinterland (southeastwards).

4.2.1 Reflector terminations to the foreland

According to basin-scale thickness and extent variations of the Eocene–Quaternary foreland tectonostratigraphic unit revealed by seismic reflectors (Figures 3, 4 and S1; Table S1), the foreland sequences can be divided into four layers. Layer 1 ranges from R24 to R46, Layer 2 from R47 to T55, Layer 3 from R56 to R137; and Layer 4 consists of all reflectors above R138 (Figure S1 and Table S1).

Layer 1, from bottom up, is composed of reflectors R24 to R46 (Figure S1). The lowermost reflector R24 laps on the top reflector R23' of the pre-foreland unit (Figure 6). The thickness of this layer stays constant from the F-K anticline, via the Kekeya syncline, to the Kekeya anticline. And it gradually thins from the northeastern limb of the Kekeya anticline to the northeastern limb of the Guman anticline (Figures 3, 4 and S1). From the northeastern limb of the Guman anticline, this layer thins rapidly, and tapers out at the middle between the Jade anticline and the Qiaokatage homocline. These observations clearly demonstrate that deposition of Layer 1 was not directly disturbed by folding. The surface geology (Wang and Peng, 2013; Lu et al., 2013; Bosboom et al., 2014a; Zheng et al., 2015) and borehole K stratigraphic column in the Kekeya anticline (Figure 5) reveal that Layer 1 is mainly composed of fine sandstone, siltstone, and mudstone. The thickness variation shown on the profile and fine sedimentary rocks indicate that Layer 1 was deposited in the middle and distal part of the foredeep depozone.

The termination of R47 is at ~283 km northeast of that of R46, indicating that the extent of R47 abruptly and significantly exceeded that of R46. Hence, R47 marks the lower boundary of Layer 2. Layer 2 includes R47 through R55. Its total thickness maintains relatively invariant from the outcrop at the northeastern limb of the F-K anticline, through the Kekeya syncline, and the Kekeya anticline, until to the Guman anticline (Figures 4 and S1). Its thickness decreases from the Guman anticline to the Jade anticline, and reaches its minimum between the Jade anticline and the Qiaokatage homocline (Figures 4 and S1). This layer maintains the minimum thickness from the Qiaokatage homocline, through the QMT, until to be cut by the Selibuya fault (Figures 4 and S1). These phenomena suggest that deposition of Layer 2 was not straightforwardly perturbed by growth of folds and thrusts involving this layer. Its thickness and lithology (Wang and Peng, 2013; Lu et al., 2013; Jia et al., 2004; Zhang et al., 2004) variations indicate that it was deposited beyond the foredeep depozone. We regarded the extent of the minimum thickness of this layer as forebulge and backbulge depozones.

Layer 3, the thickest one of this unit, ranges from R56 to R137 (Figure 4 and S1), and maintains a constant thickness from the core of the Kekeya syncline to the Guman anticline. From the Guman anticline to the Jade anticline, this layer slightly thins northwards. From the Jade anticline to the Selibuya fault, it considerably thins northwards (Figures 4 and S1). In the northeast of the Selibuya fault, this layer thins to its minimum thickness and only includes few reflectors extending beyond the profile. These observations indicate that deposition of the part of Layer 3 north of the Kekeya anticline was not disturbed by growth of the Kekeya anticline. This layer is mainly composed of gritstone and conglomerate at the outcrop of the northeastern limb of the F-K anticline (Wang and Peng, 2013), sandstone drilled at the Kekeya anticline (Figure 5; Jia et al., 2004; Zhang et al., 2004), fine sandstone and siltstone at the Mazatage hills (Sun et al., 2011). The thickness and lithology variations suggest that the wedge top depozone extends from the northeastern limb of the F-K anticline to the Guman anticline, the foredeep depozone spread from the Guman anticline to the Selibuya fault. The Selibuya fault, the southern boundary of the Bachu uplift, was inverted to a reverse fault, and caused the upper part of this formation to be eroded during deposition of the middle part of the Artux Formation of Layer 3. We suppose that the Selibuya fault was not a part of the western Kunlun orogenic belt, but an isolated reverse fault in the stable Tarim Block.

Layer 4 comprises only the Xiyu Formation ranging from R138 to the top most reflector R158. This layer occurs in the northeast of the Kekeya anticline, but absent on the crest of the Jade anticline (Figures 4 and S1). Layer 4 is mainly of conglomerate at the northeastern limb of the F-K anticline (Wang and Peng, 2013), sandstone, and siltstone at the Mazatage (J. Sun et al., 2009; D. Sun et al., 2011). Deposition of the part of Layer 4 south of the Jade anticline was explicitly disturbed by the growth of the Kekeya, the Guman and the Jade anticlines. In other words, this part was the wedge-top depozone. And deposition of the part north of the Jade anticline was not perturbed by the growth of folds, and this part is interpreted to be the foredeep depozone.

Overall, Layer 1 of the foreland unit accumulated in the proximal foredeep, and the extent of Layer 2 exceeded sharply significantly the foredeep. And Layers 3 and 4 deposited in the entire foreland basin system, but the southern boundary of the wedge top depozone of Layer 4 migrated northeastwards by an anticline zone (the Kekeya anticline) with respect to Layer 3 (Figures 4 and S1). These observations indicate that the western Kunlun foreland basin progressively migrated northeastwards.

#### 4.2.2 Reflector terminations to the hinterland

Some seismic reflectors terminate to the southwest (to the hinterland) in the profile due to tilting, and subsequent erosion (Figures 4a and S1); this type of reflector ends is termed erosion termination. Other reflectors buttress on the northeast limb of anticlines to terminate, which is termed sedimentary pinch-out. The reflectors beneath R55 terminate southwestwards due to erosion at the northeastern limb of the F-K anticline. The reflectors from R56 to R78 buttress on R55 southwestwards (Figure S1 in SI). At the crest of the Kekeya anticline, R79 and its overlaying reflectors very likely terminate southwestwards due to sedimentary pinch-out. Based on the relatively constant thickness and consistent strata dips, we speculate that R88 is the uppermost reflector at the Kekeya anticline. The thickness of the strata from R80 to R88 maintains constant in the Kekeya anticline area, so, we deduce that these reflectors were eroded to terminate at the northeast limb of this anticline. Hence, we infer that the reflectors from R88 to R137 terminate southwestwards due to the sedimentary pinch-out. The reflectors above R137 distinctly lap on the northeastern limb of the Kekeya anticline (Figure S1). The reflectors above R126 are folded to uplift, and subsequently eroded at the crest of the Jade anticline (Figure S1). Overall, the hinterland sedimentary pinch-out sites of seismic reflector gradually migrate to the foreland.

### 4.3 Chronological control of seismic reflectors

Ages of the western Kunlun foreland sequences have been well constrained by magnetostratigraphic (Sun and Liu, 2006; Sun et al., 2009; Sun et al., 2011; Zheng et al., 2015), biostratigraphic (Bosboom et al., 2014a), and radioisotope dating (Zheng et al., 2015) studies. Zheng et al.'s (2015) magnetostratigraphic section at the northern limb of the F-K anticline is ~5 km west of the southwestern segment of the seismic profile (Figure 1b); and Bosboom et al.'s (2014a) section at the northern limb of the western extension of the F-K anticline (Figure 1b) is ~35 km west of the seismic profile. The ~6850-meter-deep borehole K is near our seismic profile, and at the crest of the Kekeya anticline (Figure 1b). Given that the Kekeya (Zheng et al., 2015), and the Aertashi (Bosboom et al., 2014a) sections are closest to the seismic profile as well as borehole K, and have several reliable anchoring points, we correlated these age constraints with the stratigraphic column of borehole K, and then with the traced reflectors based on borehole logging data, and synthetic seismograms of borehole K. Five matching boundaries between the stratigraphic column of borehole K, and the sections were correlated (Figure 5).

The first correlating boundary concerns the transition from the carbonate rocks to the mudstone. At the depth of ~6316.5 m in borehole K stratigraphic column, the lithology changes from the carbonate rocks of the Kalataer Formation to the mudstone (Figure 5); and in the Aertashi section, the lithology has identical change at ~0 meter (Figure 5). These two transitions match well. This matching transition corresponds to an age of ~41.16 Ma according to Bosboom et al.'s (2014a) study. At the depth of ~5449 m in borehole K column (Figure 5), the lithology changes from mudstone intercalated with sandstone to sandstone intercalated with mudstone. These identical transitions occur at ~736.9 m of the Aeratshi section, and at ~470.5 m of the Kekeya section. This is the second correlative boundary. This lithological transition was dated at ~33.01 Ma according to the magnetostratigraphic studies (Zheng et al., 2015; Bosboom et al., 2014a). The third correlative boundary is the transition from silty mudstone to sandstone at the depth of ~4238.3 m of borehole K column (Figure 5), which matches the identical transition at ~1694 meter of the Kekeya section (Figure 5) dated at ~27.00 Ma according to Zheng et al.'s (2015) study.

The lithology transition from sandstone to conglomerate of the Kekeya section was explained as a disconformity with a hiatus of ~6.84 Myr from ~22.00 Ma to ~15.16 Ma (Zheng et al., 2015). The seismic image reveals that reflectors from R56 through R77 very likely buttress on R55 (Figures 3a, 4a and S1) at the northeastern limb of the F-K anticline. Moreover, the Wuluwusitang section (Figure 7) also displays this contact relationship (Zhou, 1985). The segment of the anticline from the Kekeya section to the Wuluwusitaing section trends steady south-southeast (Figure 1b), and thus can be regarded as a cylindrical fold. We assume that this segment grew synchronously by the same mechanism. Therefore, we infer that these 3 unconformities or disconformities can be taken as the same growth unconformity occurring during the same time. Based on the assumption and this deduction, we correlated the disconformity at Kekeya section with the unconformity at the Wulusuitang section, and the growth unconformity in the seismic profile. The growth unconformity ranges from R55 to R78 (Fig S1). VSP (vertical speed profiling) logging data and synthetic seismograms of borehole K reveal that the bottom (R55), and the top (R78) boundaries of the unconformity correspond to the depths of ~2462.0 m and ~466.0 m of borehole K stratigraphic column, respectively (Figure 5). Therefore, we correlated the ~2462.0 m depth of the stratigraphic column of borehole K with the bottom boundary of the hiatus, corresponding to an age of ~20.00 Ma according to Zheng et al.'s (2015) results. This presents the fourth correlative boundary.

Moreover, the natural gamma ray logging curve of borehole K displays a ~2-meter-thick mudstone bed from the depth of ~371.5 m to ~373.5 m with a significantly high natural gamma ray value of ~167 API contrasting the overlying and underlying strata (Figure 8). It is also the highest natural gamma ray value bed above the Bashibulak Formation. Considering that the volcanic tuff generally has a high natural gamma ray value, we inferred that this mudstone bed corresponds to the volcanic ash bed exposed at the Kekeya section, and dated at ~11 Ma (Zheng et al., 2015). Therefore, we obtained five matching age boundaries correlated with the stratigraphic column of borehole K.

Using these correlating results, we plotted ages versus depths of the strata drilled at borehole K to obtain a sedimentation curve (Figure 9). The curve shows five sedimentation rate values. From old to new, they are (1) ~100.99 m/Myr before ~33 Ma, (2) ~203.11 m/Myr from ~33 Ma to ~27 Ma, (3) ~355.26 m/Myr from ~27 Ma to ~22 Ma, (4) ~189.95 m/Myr from ~22 Ma to ~11 Ma, and (5) ~33.86 m/Myr after ~11 Ma. The sedimentation curve of borehole K (Figure 9) mimics a lazy "S", and is comparable to that of the classic foreland basin (DeCelles and Giles, 1996), suggesting that borehole K site has gone through each depozone of the western Kunlun foreland basin.

Afterwards, according to the VSP logging data and the synthetic seismograms of borehole K, these five boundaries were correlated to R23, R29′, R43, R55 and R82 (Figure 5). Ages of the reflectors are ~41.16 Ma, ~33.01 Ma, ~27.00 Ma, ~20.00 Ma, and ~11 Ma, respectively. For strata between them, we interpolated their ages. And for strata above the volcanic ash bed, we extrapolated their ages by assuming that the age of the top most bed in the present foredeep depozone with active sedimentation is zero. Accordingly, each traced reflector is correlated to a stratum age (Table S1). As such, reflectors R24, R47, R127, and R137 correspond to ~40 Ma, ~25.39 Ma, ~5.24 Ma, and ~4.07 Ma, respectively (Table S1).

## 5 Discussion

Active thrusting and folding of the western Kunlun foreland fold-and-thrust belt (e.g., He et al., 2016; Lu et al., 2016; Guilbaud et al., 2017), GPS measurements (Gan et al., 2007; Liang et al., 2013; Wang et al., 2017; Wang and Shen, 2020), and the south-dipping Tarim lithosphere (Gao et al., 2000; Kao et al., 2001) indicate that the Tarim lithosphere underthrusts beneath the western Kunlun range. In addition, the continuous northern migration of the western Kunlun foreland basin offers an opportunity to quantify the underthrusting. The seismic reflection profile is nearly perpendicular to the main segment of western Kunlun (Figure 1b). Hence, we suppose that the migration of the foreland basin derived from the profile can reflect the evolution of the foreland basin along with western Kunlun. With underthrusting of the underlying plate, each point of it successively goes through a foreland basin system from the backbuldge through forebuldge, foredeep, and the wedge-top depozones. The sedimentation rates above this point changes with its position relative to the foreland basin system, with the highest one in the foredeep, the lower one in the forebuldege, and the wedge-top. The sedimentation curve of the point mimics a lazy “S” overall (DeCelles and Giles, 1996). The sedimentation curve at borehole K (Figure 9) is consistent with that of a classic foreland basin (DeCelles and Giles, 1996). This suggests that our correlating ages of the foreland sequences (Table S1) are admissible and viable. Consequently, the ages of the foreland sequences were correlated to seismic reflectors (Table S1 and Figure S1). Therefore, based on the architecture of the infilling sequences and their ages, we can retrieve the migration of the foreland basin with the underthrusting of the Tarim lithosphere, the initiation of the foreland basin, the initiation time of its coupling with the orogenic belt as well as the ponding time of the Tarim Basin.

### 5.1 Migration of the foreland basin due to the underthrusting of the Tarim lithosphere

All reflectors terminate towards the foreland except that R127, R129, R137-2, R142, and R147 extend northeastwards beyond the profile (Figure S1). Reflector terminations to the foreland are classified as fault-cut termination, erosion termination and pinch-out types. Reflectors R47, R55, R62, R65, R68, R72, R75, and R76 are cut by the Selibuya fault to terminations (Figure S1). Reflectors R78, R80, R82, R83, R84, R85, R88, R91, R92, R95, R99, and R101 are tilted by the underlying Selibuya fault, and eroded to termination (Figure S1). The fault-cut, and erosion terminations are attributed to the growth of the local structures, e.g., the Selibuya fault. The other 135 reflectors above R23' pinch out forelandwards (Figure S1 and SI text).

Although terminations of seismic reflectors go back and forth with time (Figures 3, 4, 10 and S1), they migrate to the foreland overall. The termination of a seismic reflector to the foreland represents the distal end of deposition at that time. Generally, the thinnest sedimentary sequences or no sediments occur in the forebuldege of a foreland basin system, and thicken to the foredeep (DeCelles and Giles, 1996). Accordingly, the envelope of the distribution area of forelandward reflector terminations denotes the boundary between the foredeep and the forebulge. Thus, the migration of the boundary relative to the underlying plate can reflect that of a foreland basin (Figures10b and 10c). To quantify the migration of the western Kunlun foreland basin, we plotted the ages of strata represented by reflectors vs. the distances between reflector terminations and western Kunlun (the core of the Kekeya anticline). Although the distribution areas of lower boundaries of reflector terminations are not distinct, those of the upper boundaries are unambiguous as the upper envelop of the distribution area of reflector terminations apparently retreats toward the orogen by about 100 km from ~40 Ma to ~30 Ma (Figure 10a). Similarly, the pinch-out of the Keziluoyi Formation is at ~31 km southwest of the Wulagen and Bashibulak Formations (Figures 4 and S1). The upper envelope of the distribution area of reflector terminations after ~30 Ma demonstrates that the sedimentary boundary gradually migrated toward the foreland with time (Figure 10a). To further quantify the migration, we selected the most-distal reflector terminations within every one million years to fit an equation to quantify the migration of the western Kunlun foreland basin. The selected terminations are linked by the dashed fold line in Figure 10a. The linear fitting of the upper envelop gives an equation of $y=8.18x+276.12$, with a correlation coefficient of $R^2=0.75$. From the deposition time of R24, the lowermost, oldest reflector of this unit, to that of R149, the farthest one away from the range, the foredeep has migrated forelandwards by ~119 km over a ~40 Myr time interval (Figures 4, S1 and 10a). The linear fitting equation of the upper envelop since ~30 Ma provides an average northeastward migration rate of ~8.18 mm/yr of the foreland basin.

In an orogen-foreland basin system, buildup of the orogenic wedge can cause flexure of the underlying plate to form a foreland basin, and migration of the forebuldge to the foreland (Figure10b) (DeCelles and Giles, 1996). Furthermore, underthrusting of the underlying plate beneath the orogen may lead to migration of the foreland basin to the foreland. Thus, the migration of the foreland basin consists of the propagation of an orogenic wedge, and the underthrusting of an underlying lithosphere (Figure 10b; DeCelles and Giles, 1996; DeCelles and DeCelles, 2001; DeCelles, 2012). In other words, the migration of the foreland basin is indicative of the underthrusting of the underlying lithosphere. The upper envelop of the reflector terminations is an agent of the migration of the foreland basin.

Our analysis of the profile demonstrates that the forebuldge of the western Kunlun foreland basin system gradually retreated to the hinterland from ~40 Ma to ~30 Ma. The corresponding change in formations is the southwestward migration of the pinch-out of the Keziluoyi Formation relative to the underlying Wulagen and Bashibulak Formations. The width of a foreland basin depends on the flexural rigidity of the elastic underthrusting lithosphere (Beaumont, 1981). In contrast, a foreland basin over a viscoelastic lithosphere narrows through time during the early stage of the buildup of an orogen-basin system (Quinlan and Beaumont, 1984); correspondingly, the forebuldge migrates to the hinterland. Alternatively, changes in the effective elastic thickness of the underlying lithosphere, and the tectonic load of the associated orogenic wedge can also cause migration of the forebuldge (Turcotte and Schubert, 2002). However, significant changes in the effective elastic thickness of the underthrusting Tarim lithosphere, and tectonic load of western Kunlun were not documented, and the northern movement of the Indian plate is relatively constant during this time-span (Molnar and

Tapponnier, 1975). Additionally, the pre-foreland basin substratum was not eroded during the northward migration of the western Kunlun foreland (Figures 3 and S1), suggesting that the forebuldge was weak in amplitude with the high viscoelasticity of the lithosphere (Quinlan and Beaumont, 1984). Hence, we infer that the most likely reason for the retreat of the western Kunlun foreland basin is that the Tarim lithosphere is viscoelastic.

The upper envelop of the distribution area reveals that the foreland basin migrated forelandwards at ~8.18 mm/yr since ~30 Ma. This is also the rate of the Tarim lithosphere underthrusting beneath western Kunlun. This stable underthrusting rate indicates that the current orogenic belt, and basin configuration has been established, as also supported by stratigraphy, detrital zircon, and whole-rock geochemistry studies (Cao et al., 2014), and a steady exhumation rate of ~0.9 km/Myr from the Late Oligocene to the Early Miocene (Cao et al., 2015).

During activity of the Selibya fault from ~12.72 Ma (the correlated age of R78, the uppermost reflector cut by the fault; Table S1) to ~8.73 Ma (the correlating age of R103, the lowermost reflector overlying reflectors tiled by the fault; Table S1), the upper envelop of the termination distribution area does not change significantly (Fig 10a). Therefore, the effect of activity of the Selibuya fault on the migration of the forebulge of the western Kunlun foreland basin is negligible.

The active tectonics (Lu et al., 2016; Guilbaud et al., 2017) reveals that the underthrusting of the Tarim lithosphere is still ongoing. GPS measurements reveal that the western Kunlun front and the northern Tarim Basin (Keping, Xinhe and Kuche area) moves northeastwards with respect to the stable Eurasia plate at ~20 mm/yr, and ~14.3–~16.2 mm/yr, respectively (Gan et al., 2007; Liang et al., 2013; Wang et al., 2017; Wang and Shen, 2020). The velocity difference between them is ~3.8–~5.7 mm/yr, which can be treated as the present-day crustal shortening rate in the western Kunlun foreland fold-and-thrust belt. If this inference of GPS measurements represents the long-term shortening, the difference of ~4.4–~2.5 mm/yr between this shortening rate and the Tarim lithosphere underthrusting rate of ~8.18 mm/yr would suggest the latitudinal propagation rate of western Kunlun, i.e., a lateral growth rate of the northwestern Tibetan Plateau.

5.2 Initiation of the western Kunlun range

The base of this middle Eocene–Quaternary foreland unit is the lower limit of the Wulagen Formation, which corresponds to R24 lapping northeastward on R23' (Figures 6 and S1), correlated with ~40 Ma (the middle Eocene; Table S1). As the foreland basin moves forelandwards with the underthrusting of the underlying lithosphere at the same rate, the foreland basin filling sequences can be incorporated into the orogenic wedge, and eroded (DeCelles and Giles, 1996; Naylor and Sinclair, 2008; Sinclair and Naylor, 2012; DeCelles, 2012). The surviving oldest strata may be younger than the initial sedimentary records. The basal part of the Wulagen Formation is the oldest infilling sequence identified in the western Kunlun foreland basin. We cannot exclude the possibility that some strata older than it could have ever occurred. Accordingly, we speculate that the initiation of the middle segment of the western Kunlun range probably slightly predated the deposition time of the surviving bottom boundary of the Wulagen Formation, i.e., ~40 Ma (the middle Eocene). This result is based on the basin-scale analysis of the lowermost of the foreland basin sequences. It is worth noting that local outcrops exposed in the western Kunlun front may be not the lowermost part. Studies based on these local outcrops may find younger initiation of western Kunlun (e.g., Jin et al., 2003; Cao et al., 2015). Alternatively, along the ~700-km-long western Kunlun range, it is unknown whether initiations of each segment of the range are synchronous or diachronous. More investigations are needed to constrain its initiation.

### 5.3 Ponding of the Tarim Basin

Layer 1 of the foreland unit deposited in the foredeep, and lapped on its underlying Kalataer Formation, and all the reflectors within this layer end up northeastwards due to sedimentary tapering out (Figures 3, 4 and S1). The bottom reflector R24 laps on the top reflector R23' of the pre-foreland basin substratum, which extends to the Selibya fault, and is not eroded (Figures 3, 4 and S1). If the foredeep was underfilled, the pre-foreland basin substratum should be eroded. These observations suggest that the foreland basin was in equilibrium of subsidence-filling. At this moment, the Pamir and ancient Tian Shan was not yet in contact (Bosboom et al., 2011; 2014a; 2014b) and sediments sourced from western Kunlun can be transported away from the Tarim Basin. However, the extent of Layer 2 exceeded Layer 1 abruptly and significantly (Figures 4 and S1), indicating that the filling state of the western Kunlun foreland basin changed from a subsidence-infilling equilibrium to an overfilled state. This may be explained by a scenario where the sediments supply rate increased, and/or sediments beyond the subsidence space were not transported away from the Tarim Basin anymore. During the deposition of Layer 2, the sedimentation rate did not change (Figures 9 and 10a). However, no evidence supports the increase in the sediments rate during this period. Nevertheless, the underthrusting of the Tarim lithosphere beneath western Kunlun may lead to progressively narrowing the corridor between western Kunlun and ancient Tian Shan (Charvet et al., 2011; Chen et al., 2011), until they collided to close the corridor. Its closure caused all the sediments sourced from the ranges surrounding the Tarim Basin to be trapped, and accumulate within it. Consequently, we interpret the abrupt, significant increase in the extent of Layer 2 relative to that of Layer 1 as the initial collision of western Kunlun with ancient Tian Shan. This interpretation implies that the modern geomorphology of the Tarim Basin, ponded by surrounding ranges, took shape since the deposition of Layer 2 (Figure 11). The bottom reflector R47 of Layer 2 (Figures 4a and S1) is correlated to ~25 Ma (the late Oligocene; Table S1), corresponding to the initial ponding time of the Tarim Basin.

Aeolian sediments appeared continuously since ~26.7 Ma (Zheng et al., 2015), which is interpreted as the desertification in the Tarim Basin (e.g., Sun and Liu, 2006; Sun et al., 2011; Zheng et al., 2015). This desertification was almost contemporaneous with ponding of the Tarim Basin, and the reactivation of ancient Tian Shan (Wang et al., 2013; Li et al., 2019), suggesting that the closure of the corridor between western Kunlun and ancient Tian Shan may be one of the reasons for the desertification of the Tarim Basin due to the blockage of the wind carrying moisture from the Atlantic (Zhang et al., 2013), and the retreat of the Para-Tethys sea (Bosboom et al., 2011; 2014b).

5.4 Changes in sedimentation rates in the foredeep

Since the deposition time of R24, i.e. ~40 Ma, the rates of reflector formation in the Eocene–Quaternary foreland unit display a stepwise change, (1) 1 reflector per million years from ~40 Ma to ~33 Ma, (2) 2–3 reflectors per million years from ~33 Ma to ~12 Ma, (3) 4 reflector per million years from ~12 Ma to ~11 Ma, and (4) 7–9 reflectors per million years since ~11 Ma (Figure 10a). Considering that the Cenozoic strata in northwestern Tarim exhibit similar velocities as shown by well logging data, we assume that each seismic reflector represents the same strata thickness. The resulting sedimentation rates in the whole western Kunlun foreland basin increased in a stepwise fashion. The effective elevation of western Kunlun, representing the tectonic load, should also show stepwise increase in synchronization with subsidence and infilling of the foreland basins due to their coupling relationship (Jordan, 1981). The stepwise increases in sedimentation rates possibly imply that western Kunlun experienced four episodes of uplift. Studies in eastern segment of the western Kunlun foreland (Jiang and Li, 2014) also indicate that episodic uplifts of western Kunlun. Accordingly, the constant sedimentation rate since ~11 Ma suggests that the tectonic load of western Kunlun reached its maximum. In other words, western Kunlun reached its currently effective elevation at ~11 Ma. The timing of the abrupt, significant increase in sedimentation rates of the western Kunlun foreland basin agrees with that of the uplift acceleration of Tian Shan (Charreau et al., 2006; Li et al., 2019, 2020), suggesting that the high elevation of the northwestern Tibetan Plateau facilitated the northward propagation of deformation.

## 6 Conclusions

The ~323.2-km-long seismic reflection profile crossing the middle segment of western Kunlun images well the infilling sequences of the foreland basin. Tracing, and analyzing of 157 seismic reflectors reveal that the infilling sequences consist of four major layers. Magnetostratigraphic results from the range front were correlated with reflectors to constrain their ages. Layer 1, from bottom up, accumulated in the foredeep, and its basal unit recorded the initiation of the western Kunlun range slightly prior to ~40 Ma. The extent of Layer 2 greatly exceeded that of Layer 1 toward the north, implying that the filling of the foreland basin changed from equilibrium to overfilling. The overfilling can be explained by the collision of western Kunlun with ancient Tian Shan that closed the corridor between them, and the Tarim Basin began to take its modern geomorphologic shape at ~25 Ma. Layer 3 and Layer 4 accumulated beyond the foreland basin, while the southwestern limit of Layer 4 migrated northeastwards by an anticline zone relative to that of Layer 3. Each depozone of the western Kunlun foreland basin migrated northeastwards over time. The reflector terminations significantly retreated to the hinterland from ~40 Ma–~30 Ma. This retreat suggests that the Tarim lithosphere behaves as a viscoelastic body. The linear fitting of the upper envelop of the distribution of reflector terminations since ~30 Ma suggests that the foreland basin migrated northeastwards at an average rate of ~8.18 mm/yr, i.e. the rate of the Tarim lithosphere underthrusting beneath western Kunlun. This underthrusting rate comprises a crustal shortening rate of ~3.8–5.7 mm/yr, and a latitudinal propagation rate of western Kunlun of ~4.4–2.5 mm/yr. The abrupt increases in sedimentary accumulation rates in the entire basin suggest that western Kunlun has reached its current elevation since ~11 Ma.


**Acknowledgments**

The manuscript benefited from discussions with Prof. Mingjie Xu. We greatly appreciate the valuable comments and insightful suggestions from Editor John Geissman, the Associate Editor, and four anonymous reviewers. This work was sponsored by National Key R&D Plan of China (Grant No.2017YFC0601402), grants 41372201 and 41672198 from the National Natural Science Foundation of China. The support to YC from LABEX VOLTAIRE (ANR-10-LABX-100-01), Région Centre ARGON, and EQUIPEX PLANET (ANR-11-EQPX-0036) is also appreciated. The supporting information on the interpretation of the seismic profile, the division of the tectonostratigraphic units, the layer division of the middle Eocene–Quaternary foreland tectonostratigraphic unit, Figure S1, and Table S1 presented in this manuscript can be found online via Mendley (https://www.mendeley.com/) at http://dx.doi.org/10.17632/s8ws6vf7wr.2.


**References**


Avouac, J.P., & Tapponnier, P. (1993). Kinematic model of active deformation in central Asia. Geophysical Research Letters, 20, 895–898. doi: 10.1029/93GL00128

Avouac, J.P., Tapponnier, P., Bai, M., You, H., & Wang, G. (1993). Active thrusting and folding along the northern Tien-Shan and Late Cenozoic rotation of the Tarim relative to Dzungaria and Kazakhstan. Journal of Geophysical Research, 98, 6755– 6804. doi: 10.1029/92JB01963

Beaumont, C. (1981). Foreland basins. Geophysical Journal of the Royal Astronomical Society, 65, 291–329. https://doi.org/10.1111/j.1365-246X.1981.tb02715.x

Bosboom, R. E., Dupont-Nivet, G., Houben, A. J.P., Brinkhuis, H., Villa, G., Mandic, O., Stoica, M., Zachariasse, W. J., Guo, Z.J., Li, C.X., & Krijgsman, W. (2011). Late Eocene sea retreat from the Tarim Basin (west China) and concomitant Asian, paleoenvironmental change. Palaeogeography, Palaeoclimatology, Palaeoecology, 299, 385–398. doi:10.1016/j.palaeo.2010.11.019

Bosboom, R., G. Dupont-Nivet, Grothe, A., Brinkhuis, H., Villa, G., Mandic, O., Stoica, M., Huang, W., Yang, W., Guo, Z., &Krijgsman, W. 2014a. Linking Tarim Basin sea retreat (west China) and Asian aridification in the late Eocene. Basin Research, 26, 621-640, doi: 10.1111/bre.12054

Bosboom, R. E., Dupont-Nivet, G., Grothe, A., Brinkhuis, H., Villa, G., Mandic, O., Stoica, M., Kouwenhoven, T., Huang, W., Yang, W., &Guo, Z.J. (2014b). Timing, cause and impact of the late Eocene stepwise sea retreat from the Tarim Basin (west China). Palaeogeography, Palaeoclimatology, Palaeoecology, 403, 101–118. http://dx.doi.org/10.1016/j.palaeo.2014.03.035

Cao, K., Xu, Y., Wang, G., Zhang, K., van der Beek, P., Wang, C., Jiang, S., & Bershaw, J. (2014). Neogene Source-to-Sink Relations between the Pamir and Tarim Basin: Insights from Stratigraphy, Detrital Zircon Geochronology, and Whole-Rock Geochemistry. The Journal of Geology, 122, 433–454. doi: 10.1086/676478

Cao, K., Wang, G.-C., Bernet, M., van der Beek, P., &Zhang, K.-X. (2015). Exhumation history of the West Kunlun Mountains, northwestern Tibet: Evidence for a long-lived, rejuvenated orogen. Earth and Planetary Science Letters, 432, 391–403. http://dx.doi.org/10.1016/j.epsl.2015.10.033

Charreau, J., Gilder, S., Chen, Y., Dominguez, S., Avouac, J.-P., Sen, S., Jolivet, M., Li, Y., & Wang, W. (2006). Magnetostratigraphy of the Yaha section, Tarim Basin (China): 11 Ma acceleration in erosion and uplift of the Tian Shan mountains. Geology, 34(3), 181-184, doi: 10.1130/G22106.1

Charvet, J., Shu, L.S., Laurent-Charvet, S., Wang, B., Faure, M., Cluzel, D., Chen, Y., & De Jong, K. (2011). Paleozoic tectonic evolution of the Tianshan belt, NW China. Science China Earth Sciences, 54, 166–184. doi: 10.1007/s11430-010-4138-1

Chen, K., Gumiaux, C., Augier, R., Chen, Y., Wang, Q., Lin, W., & Wang, S., (2011) The Mesozoic paleo-relief of the Northern Tianshan (China). Terra Nova, 23,195-205. doi: 10.1111/j.1365-3121.2011.00999.x

Cowgill, E. (2010). Cenozoic right-slip faulting along the eastern margin of the Pamir salient, northwestern China. GSA Bulletin, 122(1/2), 145–161, doi: 10.1130/B26520.1

DeCelles, P. G., & Giles, K. N. (1996). Foreland basin systems. Basin Research, 8, 105–123, doi: 10.1046/j.1365-2117.1996.01491.x

DeCelles, G., & DeCelles, C. (2001). Rates of shortening, propagation, underthrusting, and flexural wave migration in continental orogenic systems. Geology, 29, 135–138, https://doi.org/10.1130/0091-7613(2001)029<0135:ROSPUA>2.0.CO;2

DeCelles, P. G. (2012). Foreland basin systems revisited: variations in response to tectonic setting, In Tectonics of Sedimentary Basins: Recent Advances, edited by C. Busby and A. Azor, p405-426, Blackwell Publishing Ltd. doi: 10.1002/9781444347166

Deng, W., Yin, J, & Guo, Z. (1996), Basic-ultramafic and volcanic rocks in Changbu-Shuanghu area of northern Xizang (Tibet), China Science in China Serie D: Earth Sciences), 26, 296–301. https://doi.org/10.1360/zd1996-26-4-296

Gan, W., Zhang P., Shen, Z.-K., Niu, Z., Wang, M., Wan, Y., Zhou, D., & Cheng, J. (2007). Present-day crustal motion within the Tibetan Plateau inferred from GPS measurements. Journal of Geophysical Research, 112, B08416, doi: 10.1029/2005JB004120

Gao, R., Huang, D, Lu, D., Qian, G., Li, Y., Kuang, C., Li, Q., Li, P., Feng, R., & Guan, Y. (2000). Deep seismic reflection profile across juncture zone between Tarim Basin and west Kunlun Mountain. Chinese Science Bulletin, 45(24), 2281-2286, doi: 10.1007/BF02886369

Guilbaud, C., Simoes, M., Barrier, L., Laborde, A., Van der Woerd, J., Li, H., Tapponnier, P., Coudroy, T., & Murray, A. (2017). Kinematics of active deformation across the Western Kunlun mountain range (Xinjiang, China) and potential seismic hazards within the southern Tarim Basin. Journal of Geophysical Research: Solid Earth, 122, 10,398–10,426. https://doi.org/10.1002/2017JB014069

He, P., Wang, Q., Ding, K., Wang, M., Qiao, X., Li, J., Wen, Y., Xu, C., Yang, S., & Zou, R. (2016). Source model of the 2015 Mw 6.4 Pishan earthquake constrained by interferometric synthetic aperture radar and GPS: Insight into blind rupture in the western Kunlun Shan. Geophysical Research Letters, 43, 1511–1519. doi:10.1002/2015GL067140

Hsü, K., Pan, G., & Sengör, A. M. C. (1995). Tectonic evolution of the Tibetan Plateau: a working hypothesis based on the archipelago model of orogenesis. International Geology Review, 37(6), 473–508. https://doi.org/10.1080/00206819509465414

Jia, C. (Ed.). (1997). Tectonic characteristic and Petroleum: Tarim Basin, China, Petroleum Industry Press, Beijing, 1–253 (in Chinese).

Jia, C., Zhang, S., & Wu, S. (2004). Stratigraphy of the Tarim Basin and adjacent area, volume II, stratigraphic charts of sub-areas, China Science Publishing Press: Beijing, 1-516 (In Chinese with English abstract).

Jiang, X., Li, Z.-X., & Li, H. (2013). Uplift of the West Kunlun Range, northern Tibetan Plateau, dominated by brittle thickening of the upper crust. Geology, 41, 4, 439-442, doi: 10.1130/G33890.1

Jiang, X.-D., & Li, Z.-X., (2014). Seismic reflection data support episodic and simultaneous growth of the Tibetan Plateau since 25 Myr. Nature Communications, 5: 5453, doi: 10.1038/ncomms6453

Jin, X., Wang, J., Chen, B., & Ren, L. (2003). Cenozoic depositional sequences in the piedmont of the west Kunlun and their paleogeographic and tectonic implications. Journal of Asian Earth Sciences 21, 755–765. https://doi.org/10.1016/S1367-9120(02)00073-1

Jordan, T.E. (1981). Thrust loads and foreland basin evolution, Cretaceous, western United States. AAPG Bulletin, 65(12), 2506-2520. https://doi.org/10.1306/03B599F4-16D1-11D7-8645000102C1865D

Karner, G.D., & Watts, A.B. (1983). Gravity anomalies and flexure of the lithosphere at mountain ranges. Journal of Geophysical Research, 88, 10449–10477. https://doi.org/10.1029/JB088iB12p10449

Kao, H., Gao, R., Rau, R.-J., Shi, D., Chen, R.-Y., Guan, Y., &Wu, F. T. (2001), Seismic image of the Tarim basin and its collision with Tibet. Geology, 29(7), 575–578, doi: 10.1130/0091-7613(2001)029<0575:SIOTTB>2.0.CO;2

Li, C, Wang. S., & Wang, L. (2019). Tectonostratigraphic history of the southern Tian Shan, western China, from seismic reflection profiling. Journal of Asian Earth Sciences, 172, 101-114, doi: 10.1016/j.jseaes.2018.08.017

Li, C., Wang, S., Naylor, M., Sinclair, H., &Wang, L. (2020). Evolution of the Cenozoic Tarim Basin by flexural subsidence and sediment ponding: Insights from quantitative basin modelling. Marine and Petroleum Geology, 112,10407. https://doi.org/10.1016/j.marpetgeo.2019.104047.

Liang, S., Gan, W., Shen, C., Xiao, G., Liu, J., Chen, W., Ding, X., &Zhou, D. (2013) Three-dimensional velocity field of present-day crustal motion of the Tibetan Plateau derived from GPS measurements. Journal of Geophysical Research, 118, 5722–5732, doi:10.1002/2013JB010503

Lu, R., Xu, X., He, D., Liu, B., Tan, X., & Wang, X. (2016). Coseismic and blind fault of the 2015 Pishan Mw 6.5 earthquake: Implications for the sedimentary-tectonic framework of the western Kunlun Mountains, northern Tibetan Plateau. Tectonics, 35, 956–964, doi:10.1002/2015TC004053

Lu, S., Du, F., &Ren, J. (2013). Regional geology of People's Republic of China: Ayitkardinsayi (J43C002002) and Yingjisa County (J43C002003), China University of Geosciences Press Company, LTD, 1-287. (In Chinese)

Matte, Ph., Tapponnier P., Arnaud N., Bourjot L., Avouac J. P., Vidal Ph., Liu Q., Pan Y., & Wang Y. (1996). Tectonics of western Tibet, between the Tarim and the Indus. Earth and Planetary Science Letters, 142, 311-330. https://doi.org/10.1016/0012-821X(96)00086-6

Meyer, B., Tapponnier, P., Bourjot, L., Metivier, F., Gaudemer, Y., Peltzer, G., Guo, S., & Chen, Z. (1998). Geophysical Journal International, 135, 1-47, doi: 10.1046/j.1365-246X.1998.00567.x

Molnar, P., & Tapponnier, P. (1975). Cenozoic tectonics of Asia: effects of a continental collision. Science, 189, 419–426. https://www.jstor.org/stable/1740465

Naylor, M., & Sinclair, H. D. (2008). Pro- vs. retro-foreland basins. Basin Research, 20, 285–303, doi: 10.1111/j.1365-2117.2008.00366.x

Pan, Y. (1990). Tectonic features and evolution of the western Kunlun Mountain region. Scientia Geolica Sinica, 3, 224–32 (in Chinese with English abstract).

Patriat, P., & Achache, J. (1984). India-Asia collision chronology has implications for crustal shortening and driving mechanism of plates Nature, 311, 615-621. doi: 10.1038/311615a0

Quinlan, G. M., & Beaumont, C. (1984). Appalachian thrusting, lithospheric flexure, and the Paleozoic stratigraphy of the Eastern Interior of North America. Canadian Journal of Earth Sciences, 21, 973-996. https://doi.org/10.1139/e84-103

Shaw, J. H., Connors, C, Suppe, J., 2004, Seismic Interpretation of Contractional Fault-Related Folds: An AAPG Seismic Atlas, AAPG Studies in Geology #53.

Sinclair, H. D., & Naylor, M. (2012). Foreland basin subsidence driven by topographic growth versus plate subduction. GSA Bulletin, 124(3/4), 368-379. https://doi.org/10.1130/B30383.1

Sun, D., Bloemendal, J., Yi, Z., Zhu, Y., Wang, X., Zhang, Y., Li, Z., Wang, F., Han, F., & Zhang, Y. (2011). Palaeomagnetic and palaeoenvironmental study of two parallel sections of late Cenozoic strata in the central Taklimakan Desert: Implications for the desertification of the Tarim Basin. Palaeogeography, Palaeoclimatology, Palaeoecology, 300, 1-10, doi: 10.1016/j.palaeo.2010.11.015

Sun, J., & Liu, T. (2006). The Age of the Taklimakan Desert. Science, 312(16), doi: 10.1126/science.1124616

Sun, J., Zhang, Z., & Zhang, L. (2009). New evidence on the age of the Taklimakan Desert. Geology, 37(2), 159-162. https://doi.org/10.1130/G25338A.1

Tapponnier, P., & Molnar, P. (1979). Active faulting and Cenozoic tectonics of the Tien Shan, Mongolia and Baykal regions. Journal of Geophysical Research, 84(B7), 3425~ 3459. https://doi.org/10.1029/JB084iB07p03425

Tapponnier, P, Peltzer, G., Le Dain, A. Y., Armijo, R., & Cobbold P. (1982). Propagating extrusion tectonics in Asia: New insight s from simple experiments with plasticine. Geology, 10, 611–616. https://doi.org/10.1130/0091-7613(1982)10<611:PETIAN>2.0.CO;2

Tapponnier, P, Xu, Z.Q., Roger, F., Meyer, B., Arnaud, N., Wittlinger, G., &Yang, J.S. (2001). Oblique stepwise rise and growth of the Tibet plateau. Science, 294, 1671-1677. doi: 10.1126/science.105978

Turcotte and Schubert, 2002, Geodynamics, Cambridge University Press, 705 pp. 141–161.

Wang, S.-L., Chen, Y., Charreau, J., Wei, D.-T., & Jia, D. (2013), Tectono-stratigraphic history of the southern Junggar basin: seismic profiling evidences. Terra Nova, 25(6), 490-495, doi: 10.1111/ter.12063

Wang, S., & Peng, S. (2013). Regional geology of People’s Republic of China: Yecheng County (J43C003004), China University of Geosciences Press Company, LTD, 1-183. (In Chinese).

Wang, W., Qiao, X., Yang, S., & Wang, D. (2017). Present-day velocity field and block kinematics of Tibetan Plateau from GPS measurements. Geophysical Journal International, 208, 1088–1102, doi: 10.1093/gji/ggw445

Wang, M., & Shen, Z.-K. (2020) Present-day crustal deformation of continental China derived from GPS and its tectonic implications. Journal of Geophysical Research: Solid Earth, 125, e2019JB018774. https://doi.org/10.1029/2019JB018774

Xiao, W.J., Windley, B.F., Chen, H.L., Zhang, G.C., & Li, J.L. (2002). Carboniferous-Triassic subduction and accretion in the western Kunlun, China: implications for the collisional and accretionary tectonics of the northern Tibetan plateau. Geology, 30, 295-298. https://doi.org/10.1130/0091-7613(2002)030<0295:CTSAAI>2.0.CO;2

Xiao, W.J., Han, F.L., Windley, B.F., Yuan, C., Zhou, H., & Li, J.L. (2003). Multiple accretionary orogenies and episodic growth of continents: Insights from the Western Kunlun Range, central Asia. International Geology Review, 45, 303-328. https://doi.org/10.2747/0020-6814.45.4.303

Xinjiang Bureau of Geology and Mineral Resources (Xinjiang BGMR). (1993). Regional Geology of Xinjiang. Geological Publishing House, Beijing, 1-841 (in Chinese with English Abstract).

Yin, A., Nie, S., Craig, P., Harrison, T.M., Ryerson, F.J., Qian, X.L., & Yang, G. (1998). Late Cenozoic tectonic evolution of the southern Chinese Tian Shan. Tectonics 17, 1–27. https://doi.org/10.1029/97TC03140

Yin, A., & Harrison, T.M. (2000). Geologic evolution of the Himalayan–Tibetan orogen. Annual Review of Earth and Planetary Sciences, 28(1), 211–280, doi: 10.1146/annurev.earth.28.1.211

Yin, A., Rumelhart, P., Butler, R., Cowgill, E., Harrison, T., Foster, D., Ingersoll, R., Zhang,Q., Zhou, X., Wang, X., Hanson, A., & Raza, A. (2002). Tectonic history of the Altyn Tagh fault system in northern Tibet inferred from Cenozoic sedimentation. Geological Society of America Bulletin, 114(10), 1257–1295, doi: 10.1130/0016-7606(2002)114<1257:THOTAT>2.0.CO;2

Yin, A. (2010). Cenozoic tectonic evolution of Asia: A preliminary synthesis. Tectonophysics, 488, 293–325, doi:10.1016/j.tecto.2009.06.002

Zhang, S., Huang, Z., &Zhu, H. (2004). Phanerozoic stratigraphy in covered area of Tarim basin, petroleum Industry Press, Beijing, 1–300 (in Chinese)

Zhang, Z., Han, W., Fang, X., Song, C., & Li, X. (2013). Late Miocene-Pleistocene aridification of Asian inland revealed by geochemical records of lacustrine-fan delta sediments from the western Tarim Basin, NW China. Paleography, Paleoclimatology and Paleoecology, 377, 52-61, doi: 10.1016/j.palaeo.2013.03.008

Zheng, H., Wei, X., Tada, R., Clift, P. D., Wang, B., Jourdan, F., Wang, P., & He, M. (2015) Late Oligocene–early Miocene birth of the Taklimakan Desert. Proceedings of the National Academy of Sciences of the United States of America, 112(25), 7662-7667. doi: 10.1073/pnas.1424487112

Zhou, Y. (1985), Some problems concerning correlation of the Pliocene and Miocene series in southwest Tarim basin. Oil & Gas Geology, 6(3), 316-325. (In Chinese).

**Figure 1.** (**a**) Topographic map of Central Asia showing the Tibetan Plateau and other active mountain belts as responses to the India-Asia collision. The shown major faults were adopted from Yin (2010). (**b**) Geologic map of the southwestern Tarim Basin and the western Kunlun range modified from Xinjiang BGMR (1993) and Wang and Peng (2013).

**Figure 2**. Simplified Cenozoic stratigraphic chart of the western Kunlun foreland front (simplified from Jia et al., 2004; Zhang et al., 2004; Bosboom et al., 2014a, Zheng et al., 2015).

**Figure 3**. Uninterpreted seismic reflection profile crossing the western Kunlun foreland region and the southwestern Tarim Basin. This profile is composed of three segments of seismic profiles. Common Middle Points (CMP) are plotted along the top of each segment. See Figure 1b for its location and Figure S1 for its undivided high-solution and large-scale version. The right ends of Figures 3a and 3b correspond to the left ends of Figures 3b and 3c, respectively, to present the entire profile. The vertical scale approximates to the horizontal one. Figures 3a, 3b and 3c share the same vertical and horizontal scales. Figure 6 is marked in Figure 3b.

**Figure 4**. Interpretation of the seismic reflection profile and key seismic reflectors tracing lines. The right ends of Figure 4a and Figure 4b correspond to the left ends of Figure 4b and Figure 4c respectively, to comprise the whole profile. See Figure 1b for its location and Figure S1 for its undivided large-scaled version. Figures 4a, 4b and 4c correspond one-to-one to Figures 3a, 3b and 3c, respectively. The vertical and horizontal scales are the same as the ones of Figure 3. Solid circles represent seismic reflector terminations. PKBLK Fm, the Pakabulak Formation; AJ Fm, the Anjuan Formation; KZLY Fm, the Keziluoyi Formation; WLG & BSBLK Fms, the Wulagen and Bashibulak Formations; KLT, the Kalataer Formation; ATS & QMG Fms, the Aertashi and Qimugen Formations; K, Cretaceous strata; J, Jurassic strata; P, Permian strata; Pre-P, pre-Permian strata; C, Carboniferous strata; D, Devonian strata; S, Silurian strata; M & U O, middle and upper Ordovician strata; Є, Cambrian strata; Pre-Є, pre-Cambrian rocks.

**Figure 5**. Correlation between the stratigraphic column of borehole K, the Kekeya (Zheng et al., 2015) and Aertashi (Bosboom et al., 2014a) magnetostratigraphic sections. See Figure 1b for their locations. Five matching boundaries are correlated based on the comparable lithology. Referenced in the text and formation boundary reflectors are denoted to the right side of borehole K column. ATS, Aerertashi Formation; QMG, Qimugen Formation; KLT, Kalataer Formation; WLG, Wulagen Formation.

**Figure 6**. Enlarged portion of the seismic reflection profile from Figure 3b that images the reflector of R24 lapping on R23'. (a) Clear seismic profile and (b) Interpreted seismic profile. R23' represents the top boundary of the Paleocene–middle Eocene platform unit and R24 is

indicative of the bottom boundary of the middle Eocene–Quaternary foreland unit. The western Kunlun range slightly predated the deposition time of R23′.

**Figure 7**. River-cut section of the northern limb of the Fusha-Keliyang (F-K) anticline along the eastern bank of the Wuluwusitang River (modified from Zhou, 1983), showing the growth unconformity occurring in the Pakabulak Formation that supports the hiatus interpretation of the northern limb of the F-K anticline in Figures 3a and 4a. See Figure 1b for its location.

**Figure 8**. Natural gamma ray and spontaneous potential logging curves of borehole K from the depth ~300 m to ~450 m. The natural gamma ray curve shows that a ~2-meter-thick mudstone bed from the depth of ~371.5 m to ~373.5 m displays a significantly high natural gamma ray value of ~167 API, while the other mudstone beds at ~416.7 m and ~447.3 m have natural gamma ray values close to the background one. See Figures 1b and 3a and 4a for the location of orehole K and Figure 5 for its relative depth in the stratigraphic column of borehole K.

**Figure 9**. Sedimentation curve of the borehole K drilled at the crest of the Kekeya anticline almost in the seismic profile. See Figure 5 for the correlation between the borehole K stratigraphic column and timing results, and Figures 1b and 3a and 4a for the borehole K location. This curve shows that the sedimentation rates of the site increased from ~40 Ma to 22 ~Ma, decreased from ~22 Ma to ~11 Ma, and reached to its minimum since ~11 Ma, indicating that the borehole K site has swept over the foreland basin system from the distal foredeep depozone to the wedge top one. This curve is concordant with that of the classic foreland basin, suggesting that the age correlation is admissible and viable.

**Figure 10**. (a) Plot of distances from the range versus the reflector terminations and their correlating ages, and plot of seismic reflector formation rates (number of reflectors per million years) through time (the gray histogram in the lower part of Figure 10a). Open symbols indicate values measured from the crest of the Kekeya anticline to terminations on Figure S1. See Table S1 for all the measured values. The dashed fold line is a distribution envelope established by connecting the maximum values within about one million of years. The solid line is fitted by values connected by the dashed fold line. The linear fitting of the upper envelop of the distribution area of reflector terminations indicates that the western Kunlun foreland basin system migrated forelandward at a rate of ~8.18 mm/yr since ~30 Ma, consisting of the present shortening rates of ~3.8–5.7 mm/yr derived from GPS measurements (Gan et al., 2007; Liang et al., 2013; Wang et al., 2017; Wang and Shen, 2020) and the western Kunlun latitudinal propagation rate of ~4.4–2.5 mm/yr. From ~40 Ma to ~30 Ma, the foreland basin retreated toward the hinterland. The retreat of the foreland basin suggests that the Tarim lithosphere behaves as a viscoelastic body. The grey histogram at lower part of Figure 10a shows that sedimentation rate of the whole basin, represented by formations rates of seismic reflector, increased in a stepwise fashion, 1 reflector per million years from ~40 Ma to ~33 Ma, 2–3 reflectors per million years from ~33 Ma to ~12 Ma, 4 reflector per million years from ~12 Ma to ~11 Ma, and 7–9 reflectors per million years since ~11 Ma. The rates reached its maximum

and have maintained constant since ~11 Ma, suggesting that western Kunlun reached its current effective elevation at that time. (b) Migration of a classic foreland basin with the underthrusting of its underlying lithosphere. Migration of the western Kunlun foreland basin is consistent with this classic type. (c) Stratal onlaps in the foreland basin that records its lateral migration (after DeCelles, 2012). This type of onlaps has been identified in the seismic profile of Figures 3, 4 and S1.

**Figure 11**. Sketch views of the physiographical evolution of the Tarim Block since the middle Eocene (a) before 40 Ma, (b) 40 Ma – 25 Ma, (c) at 25Ma, and (d) at present. Main observations that constrain this study are from the analyses of the seismic profile of Figures 3 and S1 and its interpretation of Figure 4, and Li et al.'s (2019; 2020) work.

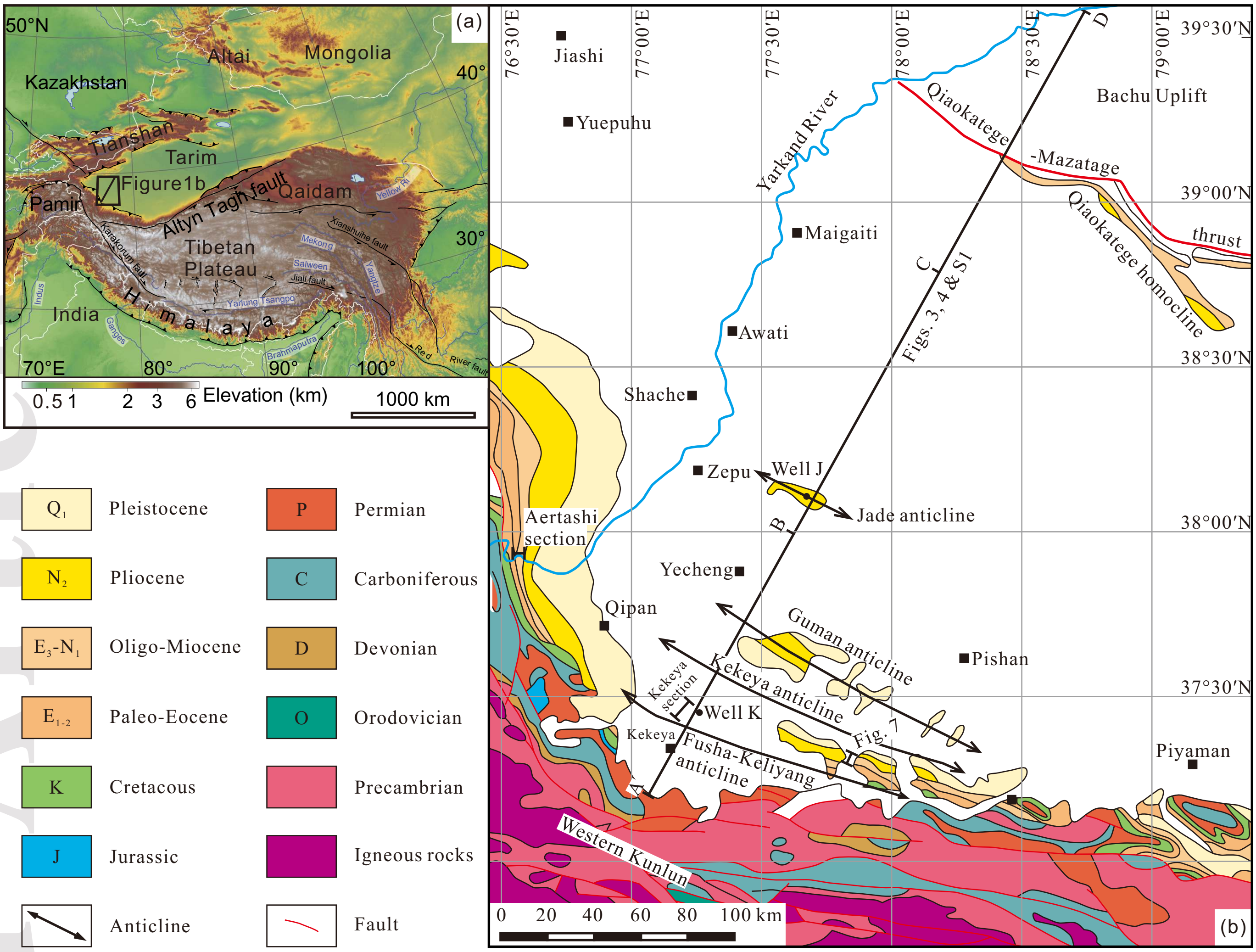
(a)
50°N
Altai
Mongolia
Kazakhstan
40°
Tianshan
Tarim
Figure1b
Pamir
Qaidam
Altyn Tagh fault
Tibetan
Plateau
30°
India
H i m a l a y a
70°E
80°
90°
100°
0.5 1 2 3 6 Elevation (km)
1000 km
Q1 Pleistocene
N2 Pliocene
E3-N1 Oligo-Miocene
E1-2 Paleo-Eocene
K Cretacous
J Jurassic
Anticline
P Permian
C Carboniferous
D Devonian
O Orodovician
Precambrian
Igneous rocks
Fault
76°30′E
77°00′E
77°30′E
78°00′E
78°30′E
79°00′E
39°30′N
39°00′N
38°30′N
38°00′N
37°30′N
Jiashi
Yuepuhu
Yarkand River
Bachu Uplift
Qiaokatege
-Mazatage
thrust
Qiaokatege homocline
Maigaiti
Awati
Shache
Figs. 3, 4 & S1
Zepu
Well J
Jade anticline
Aertashi
section
Yecheng
Qipan
Guman anticline
Pishan
Kekeya anticline
Kekeya section
Well K
Kekeya
Fusha-Keliyang
anticline
Fig. 7
Piyaman
Western Kunlun
0 20 40 60 80 100 km
(b)

| Group | Formation | Lithology in western Kunlun front | Correlating age (Ma) |
|---|---|---|---|
| | Xiyu | Conglomerate | 4.07 |
| | Artux | Siltstone, sandstone and conglometate | 18.13 |
| Wuqia | Pakabulak | Brownishi-reddish mudstione, siltstone, and thick-bedded sanstone | 22.42 |
| Wuqia | Anjuan | Mudstone, siltstone and sandstone | 27.08 |
| Wuqia | Keziluoyi | Brownish-reddish mudstone, siltstone | 33.01 |
| Kashi | Bashibulak | Reddish mudstone, siltstone and sandtome wiht some shells and gypsum beds at basal | |
| Kashi | Wulagen | Greenish mudstone with shells and gypsym beds | 41.16 |
| Kashi | Kalataer | Limestomen with intercalted mudstone,rich in shell bed and oolitics/shelly limestone | |
| Kashi | Qimugen | Massive and nodular gypsum and gypsiferous mustone, greenish-grey mudstone | |
| Kashi | Aeratshi | Massive gypsum interlayered with dolomite and mudstone | |

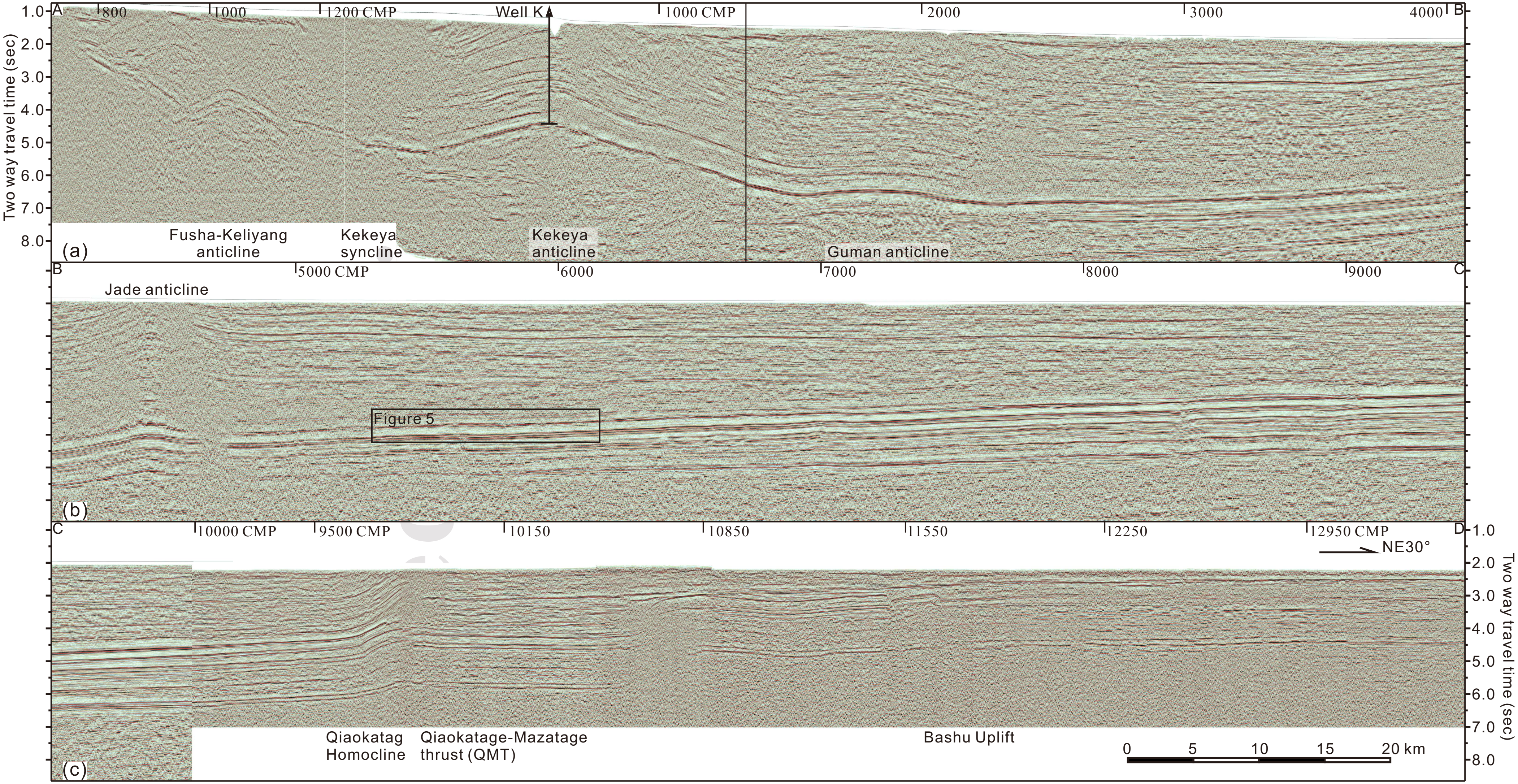

Two way travel time (sec)
1.0
2.0
3.0
4.0
5.0
6.0
7.0
8.0
A
800
1000
1200 CMP
Well K
1000 CMP
2000
3000
4000
B
(a)
Fusha-Keliyang anticline
Kekeya syncline
Kekeya anticline
Guman anticline
B
5000 CMP
6000
7000
8000
9000
C
Jade anticline
Figure 5
(b)
C
10000 CMP
9500 CMP
10150
10850
11550
12250
12950 CMP
D
NE30°
(c)
Qiaokatag Homocline
Qiaokatage-Mazatage thrust (QMT)
Bashu Uplift
0
5
10
15
20 km

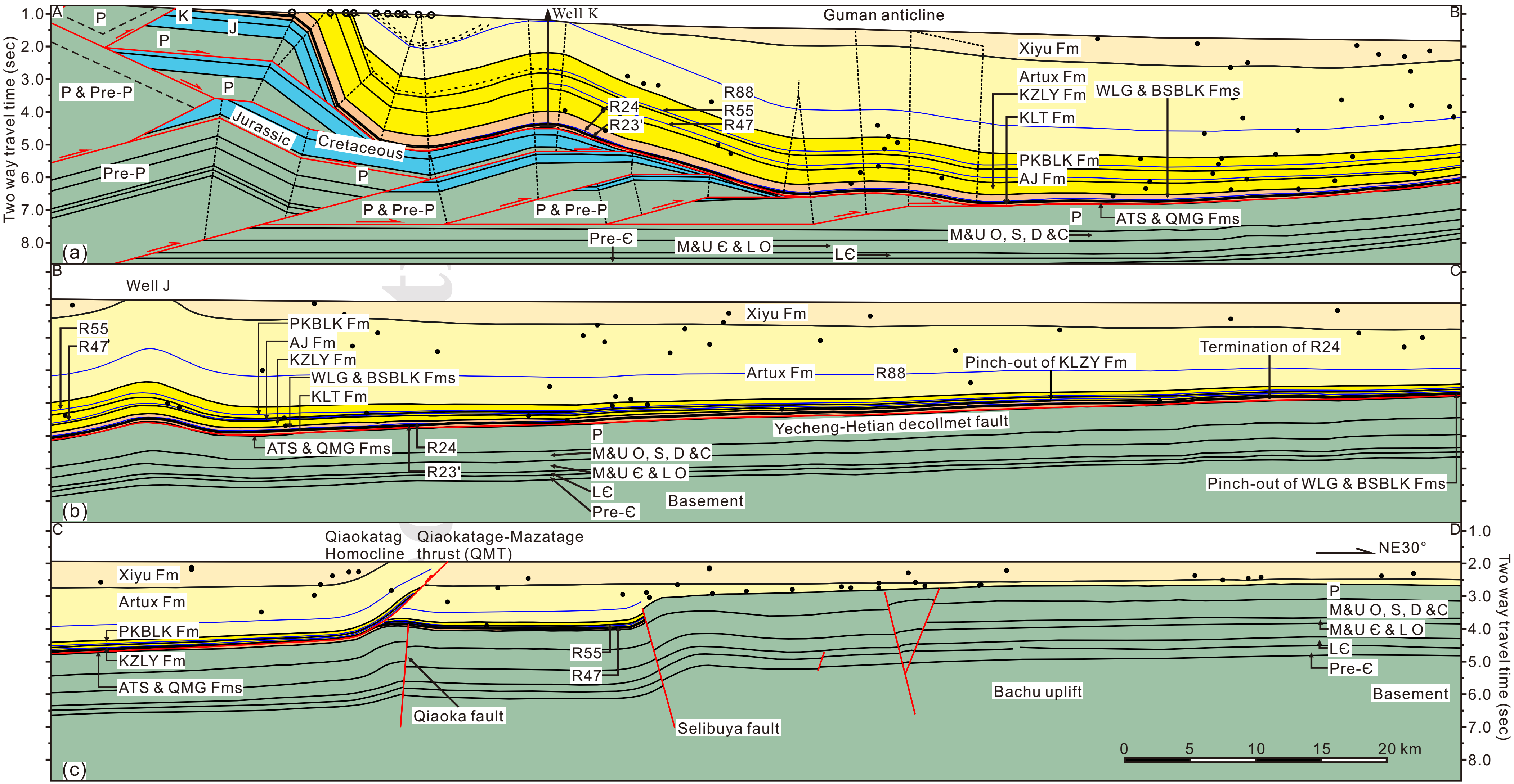

A
B
C
D
(a)
(b)
(c)
Two way travel time (sec)
1.0
2.0
3.0
4.0
5.0
6.0
7.0
8.0
Well K
Guman anticline
Xiyu Fm
Artux Fm
KZLY Fm
WLG & BSBLK Fms
KLT Fm
PKBLK Fm
AJ Fm
ATS & QMG Fms
P
K
J
P & Pre-P
Pre-P
Jurassic
Cretaceous
P & Pre-P
R88
R55
R47
R24
R23'
Pre-Є
M&U Є & L O
LЄ
M&U O, S, D &C
Well J
R55
R47'
Termination of R24
Pinch-out of KLZY Fm
Yecheng-Hetian decollmet fault
R24
R23'
M&U Є & L O
Basement
Pinch-out of WLG & BSBLK Fms
Qiaokatag Homocline
Qiaokatage-Mazatage thrust (QMT)
NE30°
Qiaoka fault
Selibuya fault
Bachu uplift
0 5 10 15 20 km

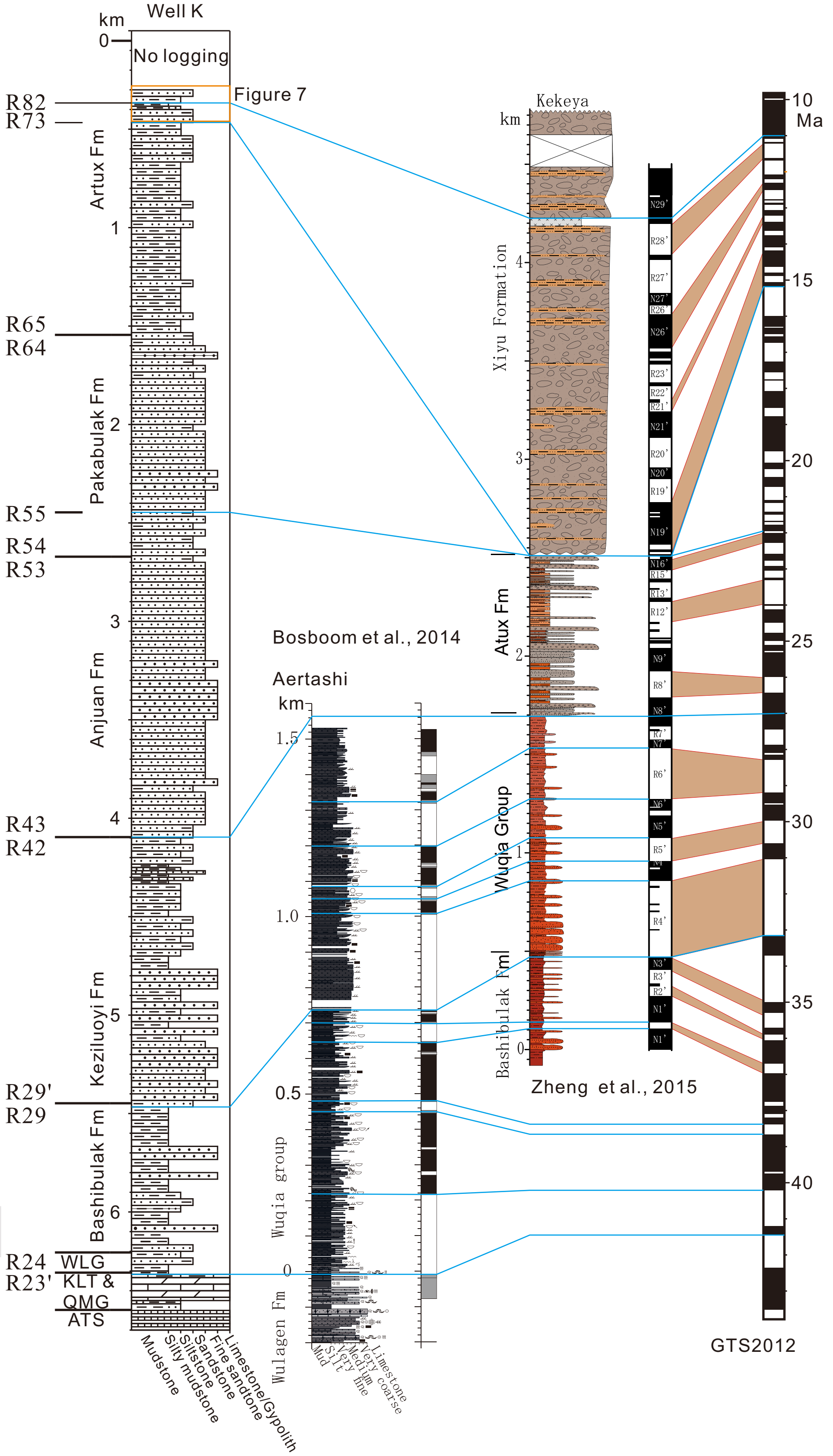

Well K
km
0
No logging
Figure 7
R82
R73
Artux Fm
1
R65
R64
Pakabulak Fm
2
R55
R54
R53
3
Anjuan Fm
4
R43
R42
Keziluoyi Fm
5
R29'
R29
Bashibulak Fm
6
R24
WLG
R23'
KLT &
QMG
ATS
Mudstone
Silty mudstone
Siltstone
Sandstone
Fine sandstone
Limestone/Gypolith
Bosboom et al., 2014
Aertashi
km
1.5
1.0
0.5
0
Wuqia group
Wulagen Fm
Mud
Silt
Very fine
Medium
Very coarse
Limestone
Kekeya
km
4
3
2
1
0
Xiyu Formation
Atux Fm
Wuqia Group
Bashibulak Fml
Zheng et al., 2015
10
Ma
15
20
25
30
35
40
GTS2012

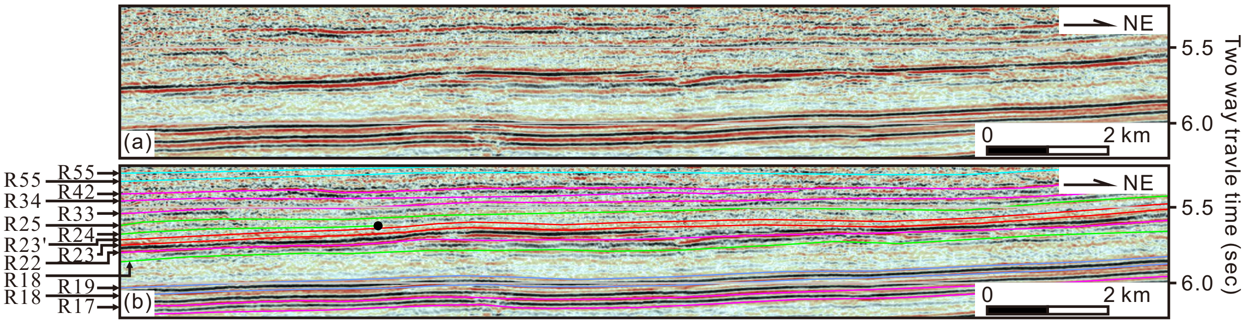

NE
5.5
6.0
Two way travle time (sec)
(a)
0
2 km
R55
R55
R42
R34
R33
R25
R24
R23'
R23
R22
R18
R19
R18
R17
(b)

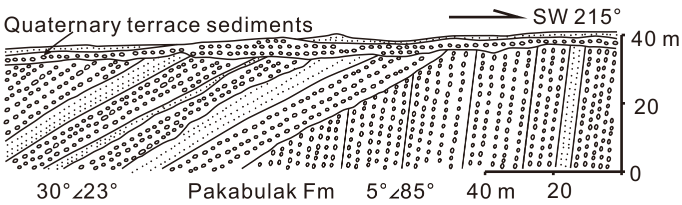
Quaternary terrace sediments
SW 215°
40 m
20
0
30°∠23°
Pakabulak Fm
5°∠85°
40 m
20

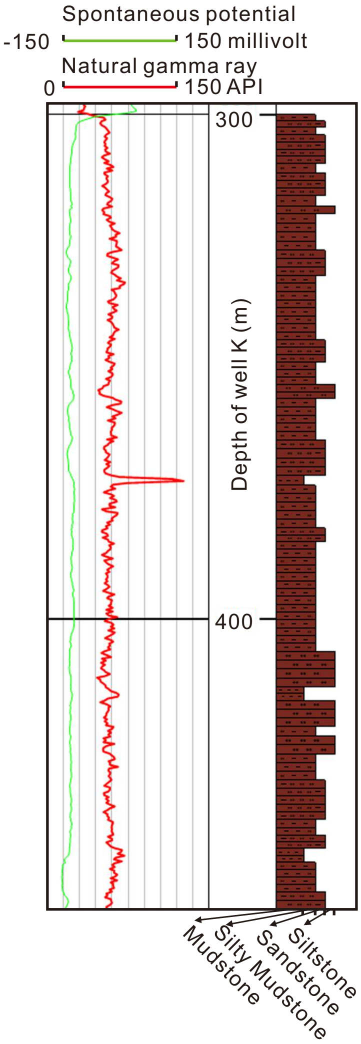
Spontaneous potential
-150
150 millivolt
Natural gamma ray
0
150 API
300
400
Depth of well K (m)
Mudstone
Silty Mudstone
Sandstone
Siltstone

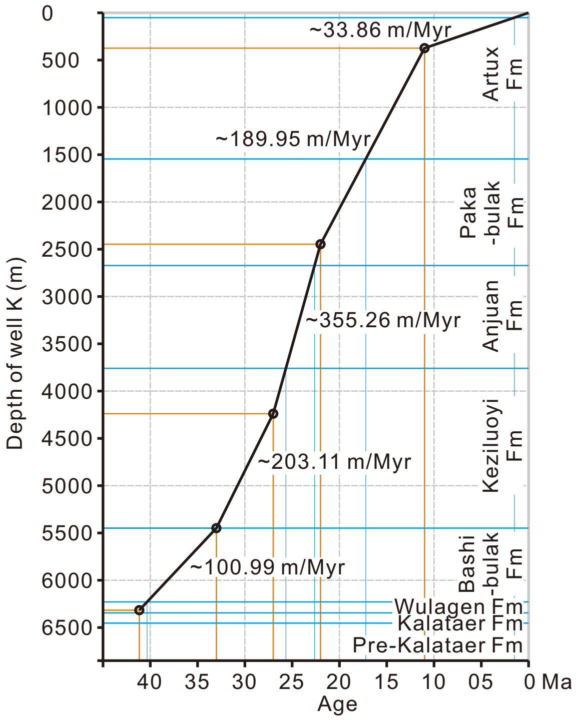
~33.86 m/Myr
~189.95 m/Myr
~355.26 m/Myr
~203.11 m/Myr
~100.99 m/Myr
Artux Fm
Paka -bulak Fm
Anjuan Fm
Keziluoyi Fm
Bashi -bulak Fm
Wulagen Fm
Kalataer Fm
Pre-Kalataer Fm
Depth of well K (m)
Age
0 Ma

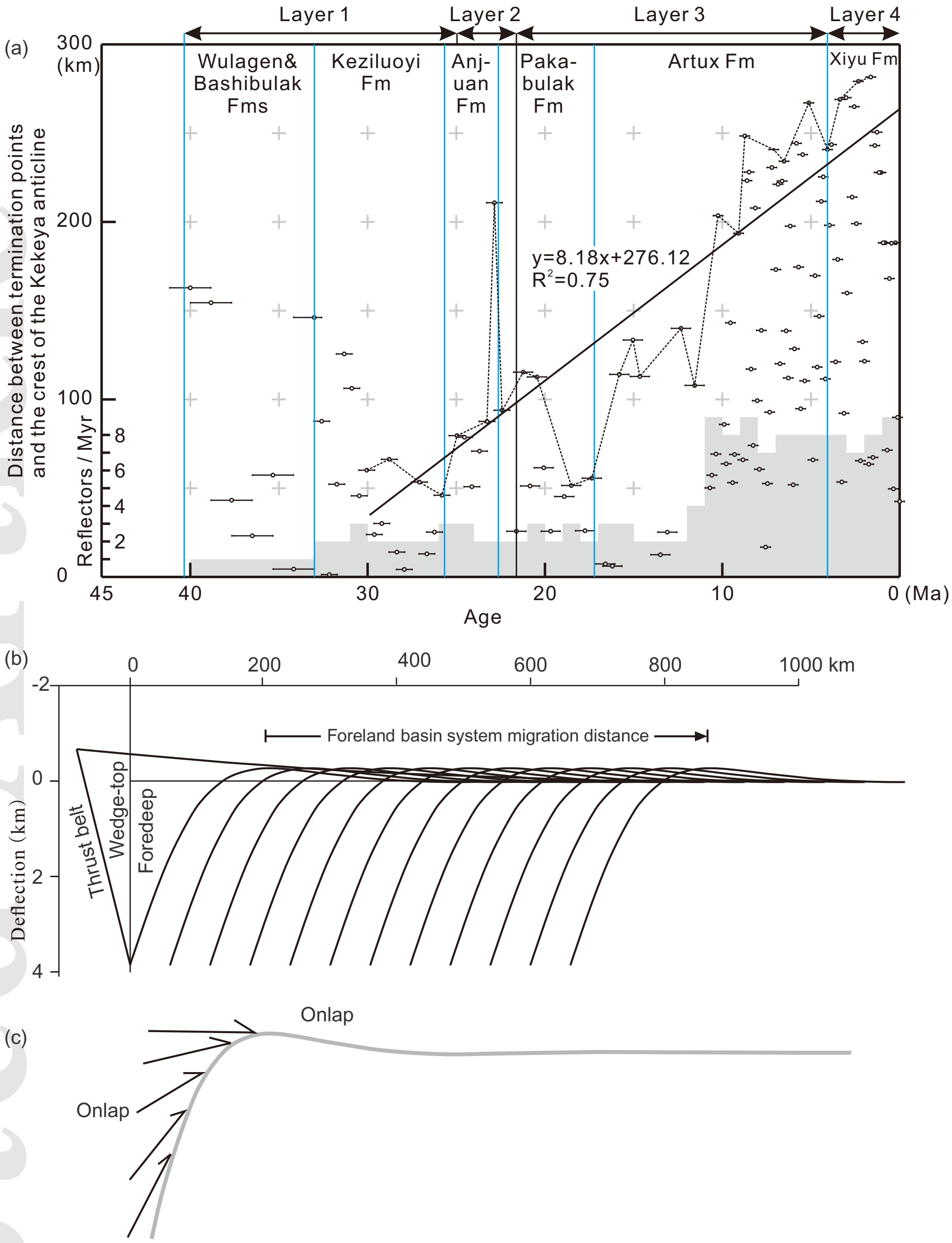
(a)
Layer 1
Layer 2
Layer 3
Layer 4
Wulagen&
Bashibulak
Fms
Keziluoyi
Fm
Anj-
uan
Fm
Paka-
bulak
Fm
Artux Fm
Xiyu Fm
300
(km)
200
100
0
Distance between termination points
and the crest of the Kekeya anticline
Reflectors / Myr
8
6
4
2
y=8.18x+276.12
R2=0.75
45
40
30
20
10
0 (Ma)
Age
(b)
0
200
400
600
800
1000 km
-2
0
2
4
Foreland basin system migration distance
Deflection (km)
Thrust belt
Wedge-top
Foredeep
(c)
Onlap
Onlap

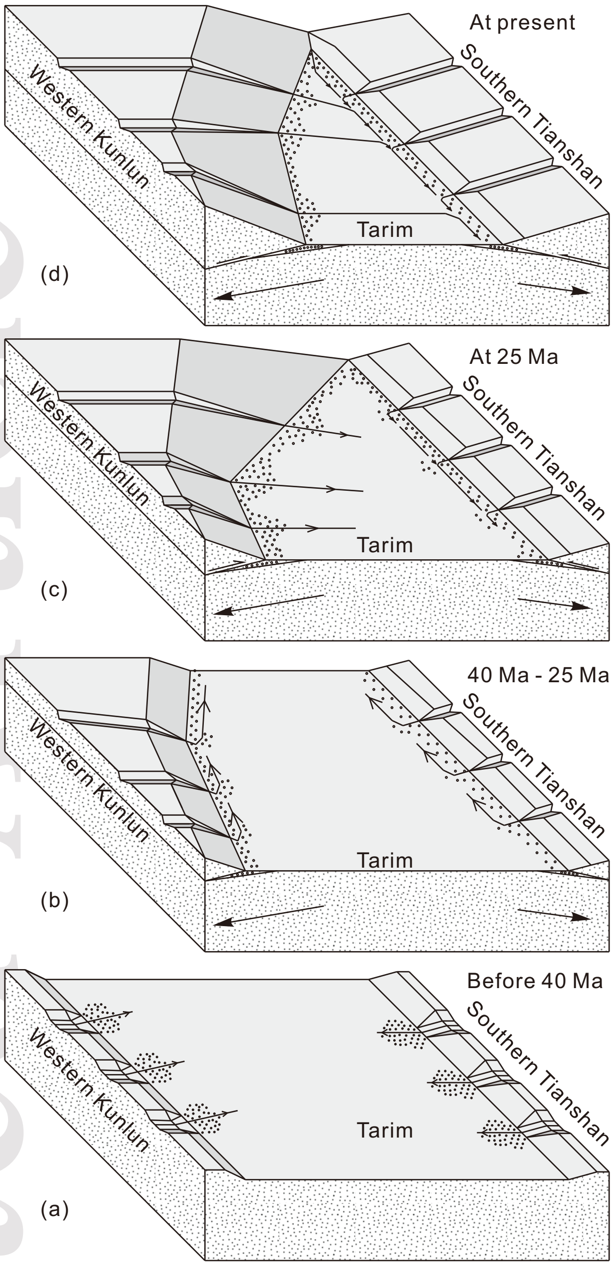
At present
Southern Tianshan
Western Kunlun
Tarim
(d)
At 25 Ma
Southern Tianshan
Western Kunlun
Tarim
(c)
40 Ma - 25 Ma
Southern Tianshan
Western Kunlun
Tarim
(b)
Before 40 Ma
Southern Tianshan
Western Kunlun
Tarim
(a)